Development of Particle Morphology in Emulsion Polymerization. 2. Cluster Dynamics in Reacting Systems

Luis J. González-Ortiz† and José M. Asua*

Grupo de Ingeniería Química, Departamento de Química Aplicada, Facultad de Ciencias Químicas, Universidad del País Vasco, Apartado 1072, 20080 San Sebastián, Spain

Received April 14, 1995; Revised Manuscript Received September 5, 1995[⊗]

ABSTRACT: A mathematical model for the development of particle morphology in emulsion polymerization has been developed. The polymer particles are considered to be a biphasic system comprising clusters of polymer 1 dispersed in a matrix of polymer 2. The model accounts for both polymerization and cluster migration. Polymerization of monomer 1 occurs both in the polymer matrix and in the clusters. The polymer 1 formed in the matrix diffuses instantaneously into the clusters. The clusters migrate toward the equilibrium morphology to minimize the free energy of the system. The driving forces for the motion of the clusters are the van der Waals interaction forces between the clusters and the aqueous phase and those between the clusters themselves. The effect of polymer matrix viscosity on the cluster motion is included. Illustrative simulations and comparisons with experimental data are presented.

Introduction

The performance of composite latex particles depends heavily on their morphology. The formation of a structured latex particle occurs through the following series−parallel processes:[1]

(a) The polymer chains are formed at a given position in a polymer particle.

(b) If the newly formed polymer chain is incompatible with the polymer already existing in the position in which it is formed, phase separation occurs. Phase separation leads to the formation of clusters.

(c) In order to minimize the Gibbs free energy, the clusters migrate toward the equilibrium morphology. During this migration, the size of the clusters may increase by (i) polymerization of the monomer inside the cluster, (ii) diffusion of polymer chains into the cluster, and (iii) coagulation with other clusters. The rates of the processes ii and iii depend strongly on the particle viscosity.

Previous theoretical approaches for the prediction of the particle morphology considered only one of the following limiting situations:

(i) The polymer chains do not move from the locus in which they are formed (with the exception of the movement due to the increase of the particle volume).[2−8]

(ii) The polymer chains are completely mobile and hence the equilibrium morphology is reached.[9−15]

However, experimental results have shown that incompatible polymer chains do move from the position in which they are formed and that in many cases, nonequilibrium morphologies are formed.[10−12,16−25] These results show that the particle morphology depends on both kinetic and thermodynamic factors.

The goal of the present series of papers is to develop a model able to predict the latex particle morphology by taking into account all the relevant kinetic and thermodynamic factors. In the first paper of the series,[1] a model for cluster migration in a nonreacting system was developed. A composite latex particle in which clusters of polymer 1 were dispersed in a matrix of polymer 2 at a temperature above the T_g's of both polymers was assumed to be the initial state. Clusters were able to move because of both van der Waals and Brownian forces. Appendix A shows that Brownian forces are negligible as compared with the van der Waals forces, and hence the actual motion of the clusters was due to the balance between the van der Waals forces and the viscous forces. The model included the calculation of the forces due to the interaction of each cluster with all the others and with the aqueous phase. Several illustrative simulations were carried out including systems for which the final equilibrium morphologies were (i) core−shell, (ii) inverted core−shell, and (iii) occluded morphology. In the present paper, the model is extended by considering that polymerization occurs concurrently with cluster migration. A future paper will also include cluster nucleation and polymer chain diffusion.

Theory

Let us consider a seeded emulsion polymerization of monomer 1 on a seed of polymer 2. Because the nucleation of the clusters is beyond the scope of this work, seed particles already containing a number of equal-size tiny clusters of polymer 1 randomly distributed in each polymer particle was taken as the initial state. The total volume of these initial clusters was negligible compared with the total amount of polymer 1 at the end of the polymerization. The monomer mass transfer rate was assumed to be high enough to maintain the monomer concentrations in the different phases at their thermodynamic equilibrium values. It was assumed that the radicals were uniformly distributed in the polymer particles; i.e., radical concentration gradients in the polymer particles were not considered. The average number of radicals per particle, $\bar{n}$, can be calculated from the balance of radicals in both the aqueous phase and the polymer particles. Because the parameters involved in these balances cannot currently be predicted, ab initio calculations of $\bar{n}$ may be uncertain. On the other hand, the exact value of $\bar{n}$ is not important in the context of this paper because the objective is to develop a general model for particle morphology. Therefore, constant values of $\bar{n}$ were used in the simulations presented in this work.

As polymerization proceeds, polymer 1 is produced in both clusters and the polymer 2 matrix. It was consid-

* To whom correspondence should be addressed.
† On leave from Universidad de Guadalajara, Guadalajara, Mexico.
⊗ Abstract published in *Advance ACS Abstracts,* November 15, 1995.

0024-9297/96/2229-0383$12.00/0

ered that the polymer 1 formed in the matrix diffused instantaneously to the clusters, the distribution of polymer 1 between clusters being proportional to the interfacial cluster−matrix area of each cluster. The size of the clusters varies because, simultaneously with polymerization, they move and coagulate due to the van der Waals forces.

The mathematical model combines the balance of forces governing the motion and coagulation of the clusters with the material balances describing the polymerization.

Cluster Dynamics. A mathematical model for the motion and coagulation of the clusters was presented in the first paper of this series,[1] where the details of the model can be found. However, to clarify the present paper, a summary of that mathematical model is presented here.

The motion of the clusters is due to the balance between the van der Waals attraction−repulsion forces and the resistance to flow that arises from viscous drag. For small movements, the equation of motion reduces to[1]

$$\mathbf{X}_j = \mathbf{X}_{j0} + \frac{\mathbf{F}_j t}{b_j \mu} \tag{1}$$

where $\mathbf{X}_j$ is the vector giving the position of cluster j, $\mathbf{F}_j$ the net van der Waals force acting on cluster j, t the time, μ the viscosity of phase 2, and b_j the friction factor of cluster j. The present paper deals with spherical and elliptical clusters (internal and superficial clusters, respectively). The friction factors for these geometries are as follows:

(i) Spherical clusters (internal clusters)[1]

$$b_j = 6\pi r_j \tag{2}$$

where r_j is the radius of the cluster.

(ii) Elliptical clusters (superficial clusters)[26]

$$b_j = \frac{32\pi((c_j/d_j)^2-1)}{\frac{2}{d_j(1-(c_j/d_j)^2)^{1/2}}\tan^{-1}\left(\frac{(1-(c_j/d_j)^2)^{1/2}}{(c_j/d_j)}\right)[2(c_j/d_j)^2-3]+2(c_j/d_j)} \tag{3}$$

where c_j is the minor equivalent semiaxis of the cluster and d_j the major one.

The net van der Waals force is given by

$$\mathbf{F}_j = \mathbf{F}_{j3} + \sum_{h=1,h\neq j}^{H} \mathbf{F}_{jh} \tag{4}$$

where $\boldsymbol{F}_{j3}$ is the force on cluster j resulting from the interaction of cluster j and phase 3, $\mathbf{F}_{jh}$ the force resulting from the interaction of clusters j and h, and H the total number of clusters. These forces can be obtained from the energies of interaction, E_j, using the following equation:

$$\mathbf{F}_j = -\nabla E_j \tag{5}$$

The energy of interaction between two bodies depends on the shape and the size of the bodies, their chemical nature, and the phase between the bodies. The shape of each cluster is the shape that minimizes the interfacial energy around the cluster. The calculation of the equilibrium morphologies, as well as the equations for the interaction energies, is given in the first paper of this series.[1] The values of the Hamaker constants required to calculate the interaction energies can be estimated from the interfacial tensions.[1]

Because the time scale for coagulation is generally much shorter than the time scale for the motion of the clusters,[1] it was assumed that instantaneous coagulation of clusters occurred when the surfaces of the clusters are closer than a critical arbitrary distance d_c.

The viscosity at near-zero shear rate was estimated as follows:[27]

$$\mu = \frac{\mu_0^* \exp\left\{\frac{E_\mu}{R}\left(\frac{1}{T}-\frac{1}{T_R}\right)\right\} C^{5.4} M^{3.4}}{C_R{}^{5.4} M_R{}^{3.4}} \tag{6}$$

where μ_0^* is the viscosity at the reference values of temperature, T_R, polymer 2 molecular weight, M_R, and concentration of polymer 2, C_R; and T, M, and C are the actual temperature, polymer 2 molecular weight, and concentration of polymer 2.

Polymerization. The material balance for monomer 1 in the reactor is

$$\frac{dM_1}{dt} = k_p \sum_i \Phi_i [M_1]_i \frac{\bar{n}}{N_A} N_p + F_{M_1} \tag{7}$$

where M_1 is the amount of monomer 1 in the reactor, k_p the propagation rate constant, Φ_i the volume fraction of phase i in the polymer particles (these phases include clusters of different size and matrix of polymer 2), $[M_1]_i$ the concentration of monomer 1 in phase i, N_p the total number of polymer particles in the reactor, N_A Avogadro's constant, and F_{M_1} the molar feed rate of monomer 1.

The balance of polymer 1 in cluster i is

$$\frac{dP_1^i}{dt} = k_p [M_1]_i \Phi_i \frac{\bar{n}}{N_A} + k_p [M_1]_m \Phi_m \frac{\bar{n}}{N_A} \frac{a_i}{\sum_{j=1}^{H} a_j} \tag{8}$$

where the first term of the right-hand side accounts for the polymer formed in the cluster, and the second for the fraction of polymer 1 formed in the matrix of polymer 2 that is transferred to cluster i. It is assumed that the distribution of the polymer 1 formed in the matrix of polymer 2 between clusters is proportional to the cluster−matrix interfacial area of each cluster, a_j.

The concentration of monomer 1 in each phase was calculated by combining the equilibrium equations and the overall material balances. Thermodynamic equilibrium is attained when the partial molar free energy of the monomer is the same in each phase. Therefore, the following equilibrium equation can be written:

$$\ln \Phi_M^{(i)} + (1-\Phi_M^{(i)}) + \chi_{Mi}(1-\Phi_M^{(i)})^2 + \frac{\Delta \bar{E}_{int}^{(i)}}{RT} = \ln\left(\frac{\Phi_M^w}{\Phi_{M,sat}^w}\right) \tag{9}$$

where $\Phi_M^{(i)}$ is the volume fraction of monomer in polymeric phase i, χ_{Mi} is the interaction parameter between the monomer and polymeric phase i, and $\Delta \bar{E}_{int}^{(i)}$ refers to the change in the interfacial energy per mole of monomer incorporated during the swelling process. The

Table 1. Change in the Interfacial Energy per Mole of Monomer Incorporated during the Swelling Process for the Different Geometries Shown in Figure 1

spherical clusters	$\frac{2\sigma_{12}V_M}{RTr_c}$
occluded clusters	$\frac{V_M}{RT}\left\{\frac{\sigma_{12}(1-\cos\theta_{12})}{R_{12}}+\frac{\sigma_{13}(1-\cos\theta_{13})}{R_{13}}\right\}$
polymer matrix	$\frac{2\sigma_{23}V_M}{RTR_{23}}$

value of $\Delta\bar{E}_{int}^{(i)}$ depends on both the geometry of the phase and the interfacial tensions. Table 1 presents the values of $\Delta\bar{E}_{int}^{(i)}$ for the geometries shown in Figure 1. The equation for occluded clusters considers that the ratio between the interfacial areas 1−2 and 1−3 remains constant during the swelling process. In addition, the presence of clusters at the surface of the polymer particle was neglected in the equation for the polymer matrix. It was checked by simulation that the effect of these assumptions on the extent of the monomer swelling was negligible.

When monomer droplets are present in the system, the right-hand side of eq 9 is equal to zero. If there are no monomer droplets, the overall material balances are needed:

$$\Phi_M^i + \Phi_{P_1}^i = 1 \tag{10}$$

$$\Phi_M^m + \Phi_{P_2}^m = 1 \tag{11}$$

$$\Phi_M^w + \Phi_W^w = 1 \tag{12}$$

$$\frac{M_1}{V_M} = V_w\Phi_M^w + \sum_i V_i\Phi_M^i + V_m\Phi_M^m \tag{13}$$

$$\sum_i P_1^i\frac{P_M}{\rho_P} = \sum_i V_i\Phi_{P_1}^i \tag{14}$$

$$V_{P_2} = V_m\Phi_{P_2}^m \tag{15}$$

$$W = V_w\Phi_W^w \tag{16}$$

where $\Phi_{P_1}^i$ is the volume fraction of polymer 1 in cluster i; $\Phi_{P_2}^m$ the volume fraction of polymer 2 in the matrix; V_M the molar volume of monomer; V_w, V_i, and V_m the volumes of aqueous phase, monomer-swollen cluster i, and monomer-swollen polymeric matrix, respectively; P_M the molecular weight of monomer; ρ_P the density of polymer 1; and V_{P_2} and W the volumes of polymer 2 and water, respectively.

The interfacial tensions depend on the extent of monomer swelling. Following Chen et al.,[11] the interfacial tension between the polymeric phases, σ_{12}, was calculated by means of the model proposed by Broseta et al.:[28]

$$\sigma_{12} = 1.334\times10^5 TM_S^{-0.875}R_g^{0.625}C_k^{-0.775}C^{1.65}\times\left\{1-0.82\left(\frac{C_k}{C}\right)^{1.55}-2\times10^{-32}M_S^{1.25}R_g^{-3.75}C_k^{-1.55}C^{0.3}\right\} \tag{17}$$

where T is the temperature, M_S the molecular weight of the polymeric system, R_g the radius of gyration, C_k the critical demixing concentration, and C the polymer concentration. The radius of gyration is proportional to $M_S^{1/2}$

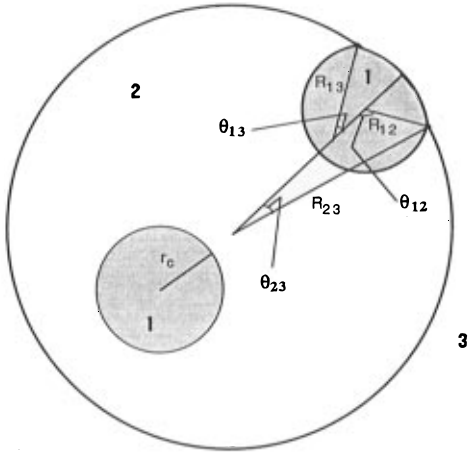

Figure 1. Geometries considered during the swelling process of each phase in the structured particle.

$$R_g = k_M M_S^{1/2} \tag{18}$$

The values of k_M were those reported in the literature for each polymer.[29]

The critical concentration of demixing can be calculated as follows:

$$C_k = AM_S^B \tag{19}$$

where A and B are empirical constants reported for each polymer−solvent system.[11,13,28]

Following Winzor and Sundberg,[13] the interfacial tensions between the polymers and the aqueous phase was calculated using the model proposed by Siow and Paterson:[30]

$$\frac{(\sigma_{i3}-\sigma_{M3}^*)a}{kT} = \ln\left(\frac{\Phi_M^{S(i)}}{\Phi_M^{(i)}}\right)+\left(\frac{r-1}{r}\right)(\Phi_P^{S(i)}-\Phi_P^{(i)})+\chi_i[0.5(\Phi_P^{S(i)})^2-0.75(\Phi_P^{(i)})^2] \tag{20}$$

$$\frac{(\sigma_{i3}-\sigma_{i3}^*)a}{kT} = \ln\left(\frac{\Phi_P^{S(i)}}{\Phi_P^{(i)}}\right)^{1/r}+\left(\frac{r-1}{r}\right)(\Phi_P^{S(i)}-\Phi_P^{(i)})+\chi_i[0.5(\Phi_M^{S(i)})^2-0.75(\Phi_M^{(i)})^2] \tag{21}$$

where σ_{i3} is the interfacial tension between phase i swollen with monomer 1 and the aqueous phase; σ_{M3}^* is the interfacial tension between monomer 1 and the aqueous phase; a is the surface area occupied by a molecule of monomer 1; $\Phi_M^{S(i)}$ and $\Phi_M^{(i)}$ are the volume fractions of monomer 1 at the surface of phase i and in the bulk of phase i, respectively; σ_{i3}^* the interfacial tension between polymer i and the aqueous phase; $\Phi_P^{S(i)}$ and $\Phi_P^{(i)}$ are the volume fractions of polymer at the surface of phase i and in the bulk of phase i, respectively; and r is the ratio of the molar volumes of polymer and monomer. For emulsion polymers, the ratio $1/r$ can be considered to be zero.

By subtraction, eqs 20 and 21 yield an equation for $\Phi_M^{S(i)}$.

$$\frac{(\sigma^*_{M3} - \sigma^*_{i3})a}{kT} + 0.75\chi_i[2\Phi_M^{(i)} - 1] + 0.5\chi_i = \ln\left(\frac{\Phi_M^{(i)}}{\Phi_M^{S(i)}}\right) + \chi_i\Phi_M^{S(i)} \quad (22)$$

Equations 9−22 are a system of nonlinear algebraic equations that were solved for each integration step of the simulation. The integration was carried out using a finite difference method in which the time interval was adjusted in such a way that no cluster was allowed to move more than 0.5 nm in one time interval.

Illustrative Simulations

The goal of this work is to develop a model including concurrent polymerization and cluster migration, but leaving the nucleation processes out of the scope of this paper. This is a burden for the illustrative simulations because an arbitrary initial state must be chosen and the evolution of the particle morphology is partially determined by the initial state. Therefore, although the current model represents a substantial improvement over the previous model[1] in which polymerization was not considered, the simulations detailed below still cannot be claimed to be accurate descriptions of a real system because such a system includes processes other than cluster migration and polymerization. Nevertheless in spite of the simplifications included in the model, it represents the first reported attempt that we are aware of to describe in a detailed way dynamic changes in the particle morphology during polymerization.

In the illustrative simulations, it will be assumed that the whole population of particles is represented by one particle. In the initial state, the particle contained 200 tiny clusters of the same size randomly distributed in the polymer particle. The total volume of these initial clusters was negligible as compared with the total amount of polymer 1 at the end of the polymerization.

Polymerizations of methyl methacrylate on a polystyrene seed using the recipes given in Table 2 were simulated. Both semicontinuou and batch polymerizations with different seed/monomer ratios were considered. In addition, different polymerization rates were simulated by using arbitrary values of $\bar{n}$ that were kept constant during each polymerization. The parameters used in the simulations are given in Table 3. The Hamaker constants were estimated from the interfacial tensions using the approach proposed by González-Ortiz and Asua.[1]

Figure 2 presents the evolution of the particle morphology for run 1 in Table 2. This run resembles closely the polymerization of MMA on a polystyrene seed using Pluronic F-108 as emulsifier reported by Chen et al.[17] The size of the phases plotted in Figure 2 corresponds to the swollen state. The monomer-swollen clusters of different sizes that appeared in the initial state resulted from the coagulation of neighbor clusters that made contact when they grew during the swelling of the initial system by the monomer. Figure 2 shows that, at the beginning of the process, the clusters, which were growing by both polymerization and coagulation, migrated toward the center of the particle. For a conversion of about 35%, an inverted core−shell morphology was predicted. As polymerization proceeded further, the morphology evolved toward the occluded morphology that was reached by the end of the process. This behavior was due to the effect of monomer swelling on the interfacial tensions that in turn influenced the Hamaker constants.[1] Figure 3 shows the evolution of the interfacial tensions during the process. It can be seen that σ_{12} increased with conversion because the higher the swelling of the different phases with monomer, the lower the interfacial tensions. On the other hand, σ_{13} and σ_{23} changed only slightly during the polymerization. Figure 4 presents the evolution of the Hamaker constants calculated from the values of σ_{ij} in Figure 3 by means of the approach presented by González-Ortiz and Asua.[1] Figure 4 shows that while the Hamaker constants governing the interaction between clusters are always positive (clusters always attract one another), A_{123} is negative at the beginning of the process (repulsion between clusters and the aqueous phase) and positive afterward (attraction between clusters and the aqueous phase).

It is interesting to compare the predictions of the present model with the particle morphologies experi-

Table 2. Recipes Used for the Simulations[a]

	batch				semicontinuous (run 5)	
	run 1	run 2	run 3	run 4	initial charge	feed
polymer seed (cm^3)	68.1	68.1	68.1	68.1	68.1	
MMA (cm^3)	143.4	68.1	32.4	68.1	3.4	64.7
water (cm^3)	788.5	863.8	899.5	863.8	863.8	
$\bar{n}$	2.5	2.5	2.5	0.5	2.5	

[a] d_p = 190 nm; $N_p = 1.9 \times 10^{16}$; T = 70 °C; feeding time, 6 h.

Table 3. Parameters Used in the Simulations

$M = 8.4 \times 10^5$ g/mol[a]	$\mu^*_0 = 5 \times 10^3$ Pa s[b]
$M_S = 1.4 \times 10^6$ g/mol[a]	$M_R = 2.5 \times 10^5$ g/mol[b]
$A = 227$[a]	$E_\mu = 7000$ J/mol[b]
$B = -0.615$[a]	$T_R = 220$ °C[b]
$R_g = 8.77 \times 10^{-6}$ cm[a]	$C_R = 1.05$ g/cm^3[b]

$$k_p = 8.7 \times 10^8 \exp\left[\frac{-4700 \text{ cal/(mol K)}}{RT}\right]\left(\frac{\text{cm}^3}{\text{mol s}}\right)^c$$

$\chi_1 = 0.95$[d]	$\sigma^*_{M3} - \sigma^*_{13} = 2.1$[d]
$\chi_2 = 1.0$[d]	$\sigma^*_{M3} - \sigma^*_{23} = 2.7$[d]

[a] Chen et al.[11] [b] Van Krevelen.[27] [c] Walling.[31] [d] Estimated by fitting the data reported by Chen et al.[11] with eqs 20−22.

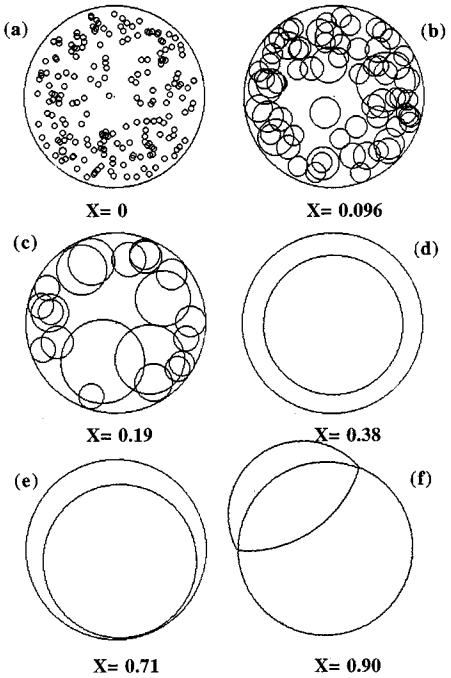

Figure 2. Evolution of the particle morphology for run 1 in Table 2. $\bar{n}$ = 2.5.

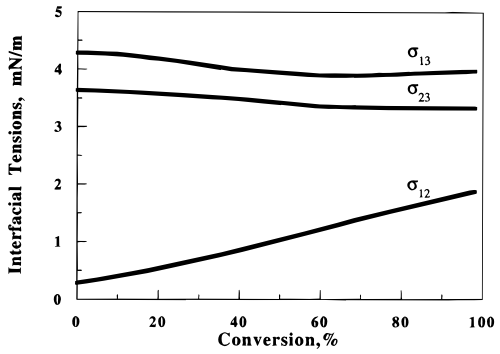

Figure 3. Evolution of the interfacial tensions during run 1 in Table 2. $\bar{n} = 2.5$.

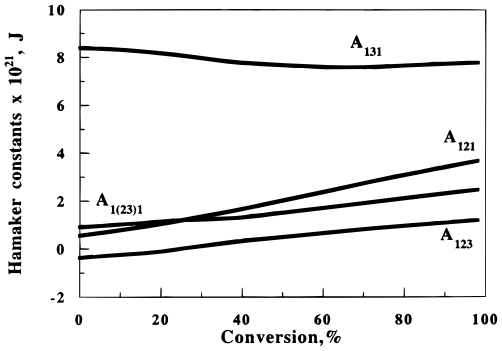

Figure 4. Evolution of the Hamaker constants during the seeded batch emulsion polymerization. $\bar{n} = 2.5$.

mentally observed by Chen et al.[17] At conversions below 20%, Chen et al.,[1] using the "embedded in ice" technique, observed (Figure 5a in ref 17) that there were many pMMA clusters close to the surface of the particle. Qualitatively, this corresponds well with the morphology presented in Figure 2c. It should be noted that the model based on the instantaneous thermodynamic equilibrium cannot be used because it predicts an inverted core−shell. At higher conversions (43%), particles in which the pMMA was almost completely covered by pSt were observed (Figure 6a in ref 17). This experimental observation agrees well with the prediction of the present model shown in Figure 2d. At even higher conversions (90%), occluded morphologies were observed (Figure 7b in ref 17), in agreement with the predictions of the model, presented in Figure 2f.

Figures 5 and 6 present the evolutions of the particle morphologies for runs 2 and 3 in Table 2. They were batch seeded emulsion polymerizations with lower monomer/seed polymer ratios than in run 1. The initial state (number and size of initial clusters) was the same as that in run 1. In runs 2 and 3, the clusters migrate toward the surface of the particle during the whole process, because for these low monomer swellings, the Hamaker constants were always positive. Comparison between Figures 2, 5, and 6 shows that the higher the monomer/seed polymer ratio, the closer the particle morphology reached at the end of polymerization is to the equilibrium morphology. There are two reasons for this behavior. First, the viscosity of the polymer matrix decreases when the amount of monomer increases, and hence the motion of the clusters was less hindered. Second, because of the high swelling ratios, the volume of the clusters exceeded the volume of the polymer matrix and the clusters made contact, leading to an extensive coagulation.

Figure 7 presents the effect of the polymerization rate (different values of $\bar{n}$) on the evolution of the particle morphology. It can be seen that the slower the polym-

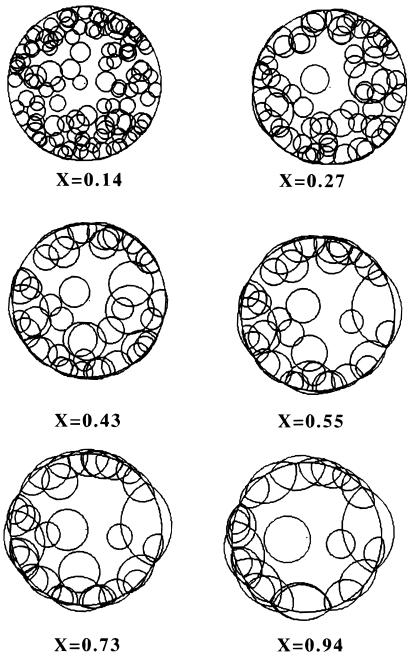

Figure 5. Evolution of the particle morphology for run 2 in Table 2. $\bar{n} = 2.5$.

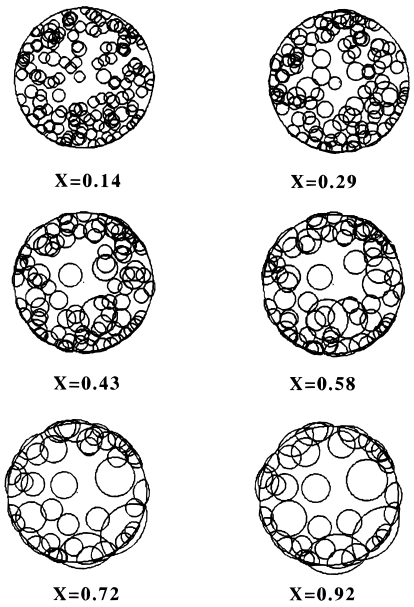

Figure 6. Evolution of the particle morphology for run 3 in Table 2. $\bar{n} = 2.5$.

erization rate, the closer the final structure of the particle to the equilibrium morphology. These results agree qualitatively well with the experimental data reported by Jönsson et al.[21] (Figures 3A and 4 in ref 21).

Figure 8 presents the evolution of the particle morphology for run 5 in Table 2. In this figure, the conversion was defined as the fraction of the total MMA in the recipe that had been converted into polymer. Under the simulated conditions, the volume fraction of polymer in the particles was in the range of 95% throughout the feeding period. It can be seen that during the whole process, the clusters migrate toward the surface of the particle. In addition, comparison with Figure 5 shows that because of the higher viscosity, the motion of the clusters in the semicontinuous process was significantly slower than in the batch process. Nevertheless, the longer process time required for the semi-

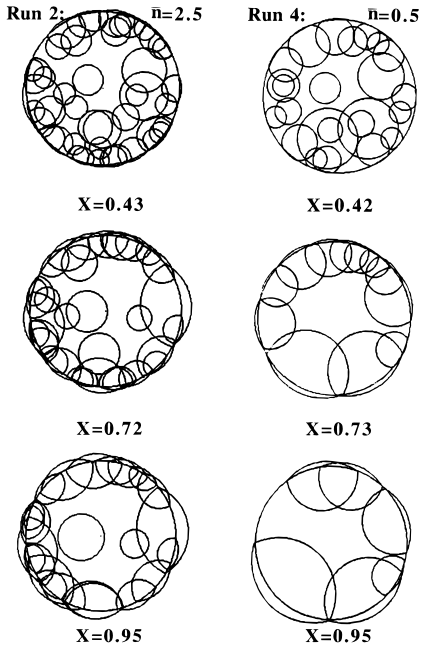

Figure 7. Effect of the polymerization rate on the evolution of the particle morphology.

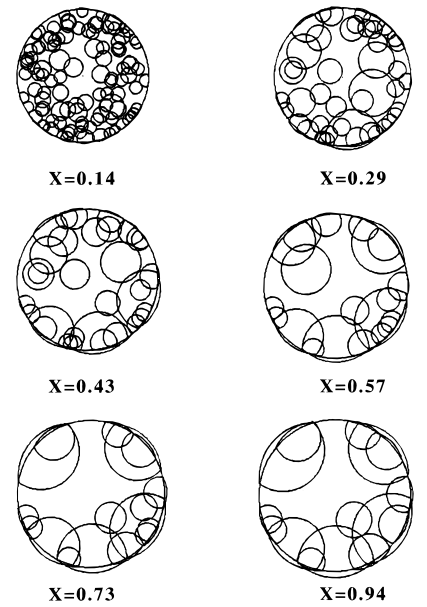

Figure 8. Evolution of the particle morphology for run 5 in Table 2. $\bar{n} = 2.5$.

continuous polymerization almost counteracted the effect of the particle viscosity.

Conclusions

In the foregoing, a mathematical model for the development of particle morphology in emulsion polymerization has been developed. The polymer particles are considered to be a biphasic system comprising clusters of polymer 1 dispersed in a matrix of polymer 2. The model accounts for both polymerization and cluster migration. Polymerization of monomer 1 occurs in both the polymer matrix and the clusters. The concentrations of the monomer in the different phases were given by the thermodynamic equilibrium. The polymer 1 formed in the matrix diffuses instantaneously into the clusters. The clusters migrate toward the equilibrium morphology to minimize the free energy of the system. The driving forces for the motion of the clusters are the van der Waals interaction forces between the clusters and the aqueous phase and those between the clusters themselves. The effect of polymer matrix viscosity on cluster motion is included. The model was used to simulate the polymerization of MMA on a polystyrene seed. It was found that, at the beginning of the process, the clusters migrated toward the center of the particle, forming an inverted core−shell morphology at intermediate conversions. Later the morphology evolved toward the occluded type. This behavior was due to the effect of the monomer swelling on the interfacial tensions that in turn influenced the Hamaker constants. These predictions agreed quite well with the experimental results reported by Chen et al.[17] Simulations showed that the final particle morphology depended heavily on kinetic factors. Furthermore, the higher the monomer/seed ratio, the closer the structure of the particle reached at the end of polymerization is to the equilibrium morphology. In addition, it was found that the slower the polymerization rate, the closer the final structure of the particle to the equilibrium morphology.

Acknowledgment. The AECI−UPV fellowship for L.J.G.-O. and financial support by the Diputación Foral de Gipuzkoa are gratefully appreciated.

Appendix A. Brownian Forces vs van der Waals Forces

The motion of a given cluster j is controlled by the following equation:

$$m_j \frac{d^2\mathbf{X}_j}{dt^2} = \mathbf{F}_j + \mathbf{F}_j' - b_j\mu \frac{d\mathbf{X}_j}{dt} \qquad \text{(A-1)}$$

where m_j is the mass of the cluster, $\mathbf{X}_j$ the vector defining the position of cluster j, $\mathbf{F}_j$ the net van der Waals force acting on the cluster, $\mathbf{F}_j'$ the random fluctuating force that takes into account the Brownian motion, μ the viscosity of the polymer matrix, and b_j the friction factor. For the systems simulated in this paper, the van der Waals forces acting on a cluster calculated by means of eq 5 are normally at least 10^{-14} N. Neither the estimation of the random fluctuating force, $\mathbf{F}_j'$, nor the comparison between random forces and directional forces is a simple task. Nevertheless, sedimentation of polymer latexes can provide some information. It is well known that for a typical polymer latex, Brownian motion only counteracts sedimentation of latexes significantly when the diameters are smaller than about 500−600 nm. This means that in this region, the effect of the random fluctuating force is similar to the resulting directional force acting on the latex particle (gravity force minus floating force). Therefore, the value of these forces is an estimate of the directional force equivalent to the random force. The resulting directional force acting on a latex particle 600 nm in diameter with density of 1.1 g/cm^3 dispersed in water is about 1×10^{-16} N. This value is at least 2 orders of magnitude lower than that of the van der Waals forces, and hence the contribution of the Brownian forces to the motion of the clusters can be safely neglected.

Nomenclature

a	surface area occupied by a molecule of monomer 1
a_j	matrix−cluster interfacial area
A	empirical constant (eq 19)
b_j	friction factor
B	empirical constant (eq 19)

C polymer concentration
c_j minor semiaxis of cluster j
C_k critical demixing concentration
C_R reference concentration of polymer 2
d_j major semiaxis of cluster j
E_j energy of interaction of cluster j
E_μ energy of activation for the viscosity of polymer solutions
$\mathbf{F}_j$ net van der Waals force acting on cluster j
$\mathbf{F}_j'$ random fluctuating force acting on cluster j
$\mathbf{F}_{j3}$ force acting on cluster j resulting from the interaction between cluster j and the aqueous phase
$\boldsymbol{F}_{jh}$ force acting on cluster j resulting from the interaction between clusters j and h
F_{M_1} molar feed rate of monomer 1
H number of clusters
k Boltzmann's constant
k_M empirical constant (eq 18)
k_P propagation rate constant
M molecular weight of polymer 2
M_R reference molecular weight of polymer 2
M_S molecular weight of the polymeric system
M_1 amount of monomer 1 in the reactor
$[M_1]_i$ concentration of monomer 1 in phase i
$[M_1]_m$ concentration of monomer 1 in the polymeric matrix
$\bar{n}$ average number of radicals per particle
N_A Avogadro's constant
N_p total number of polymer particles in the reactor
P_1^i amount of polymer 1 in phase i
P_M molecular weight of monomer
r ratio of the molar volumes of polymer and monomer
R universal gas constant
r_j radius of cluster j
R_g radius of gyration
t time
T temperature
T_R reference temperature
V_i volume of monomer-swollen cluster i
V_m volume of monomer-swollen polymeric matrix
V_M molar volume of monomer
V_{P_2} volume of polymer 2
V_w volume of the aqueous phase
W volume of water
$\mathbf{X}_j$ vector giving the position of cluster j

Greek Symbols

χ_{Mi} interaction parameter between monomer and the polymeric phase i
ρ_P density of polymer 1
$\Delta E_{int}^{(i)}$ change of interfacial energy per mole of monomer incorporated during the swelling process
Φ_i volume fraction of phase i in the polymer particles
Φ_J^k volume fraction of component J (M, monomer; P_1, polymer 1; P_2, polymer 2; W, water) in phase k (i, cluster i, m, polymeric matrix; w, aqueous phase)
$\Phi_{M,sat}^w$ volume fraction of monomer in aqueous phase at saturation
$\Phi_M^{(i)}$ volume fraction of monomer in the bulk of the polymer phase i
$\Phi_M^{S(i)}$ volume fraction of monomer at the surface of the polymeric phase i
$\Phi_P^{(i)}$ volume fraction of polymer in the bulk of the polymeric phase i
$\Phi_P^{S(i)}$ volume fraction of polymer at the surface of the polymeric phase i
μ viscosity of the polymeric matrix
μ_0^* reference viscosity
σ_{i3} interfacial tension between the monomer-swollen phase i and the aqueous phase
σ_{i3}^* interfacial tension between the polymer i and the aqueous phase
σ_{M3}^* interfacial tension between the monomer and the aqueous phase

References and Notes

(1) González-Ortiz, L. J.; Asua, J. M. *Macromolecules* **1995**, *28*, 3135.
(2) Grancio, M. R.; Williams, D. J. *J. Polym. Sci., Part A-1* **1970**, *8*, 2617.
(3) Keusch, P.; Graff, R. A.; Williams, D. J. *Macromolecules* **1974**, *7*, 304.
(4) Chern, C.-S.; Poehlein, G. W. *J. Polym. Sci., A: Polym. Chem.* **1987**, *25*, 617.
(5) de la Cal, J. C.; Urzay, R.; Zamora, A.; Forcada, J.; Asua, J. M. *J. Polym. Sci., A: Polym. Chem.* **1990**, *28*, 1011.
(6) Mills, M. F.; Gilbert, R. G.; Napper, D. H. *Macromolecules* **1990**, *23*, 4247.
(7) Yang, S. I.; Klein, A.; Sperling, L. H.; Cassasa, E. F. *Macromolecules* **1990**, *23*, 4582.
(8) Croxton, C. A.; Mills, M. F.; Gilbert, R. G.; Napper, D. H. *Macromolecules* **1993**, *26*, 3563.
(9) Torza, S.; Mason, S. G. *J. Colloid Interface Sci.* **1970**, *33*, 67.
(10) Sundberg, D. C.; Casassa, A. P.; Pantazopoulos, J.; Muscato, M. R.; Kronberg, B.; Berg, J. *J. Appl. Polym. Sci.* **1990**, *41*, 1425.
(11) Chen, Y.-C.; Dimonie, V.; El-Aasser, M. S. *J. Appl. Polym. Sci.* **1991**, *42*, 1049.
(12) Chen, Y.-C.; Dimonie, V.; El-Aasser, M. S. *Macromolecules* **1991**, *24*, 3779.
(13) Winzor, C. L.; Sundberg, D. C. *Polymer* **1992**, *33*, 3797.
(14) Durant, Y. G. J.; Guillot, J. *Colloid Polym. Sci.* **1993**, *271*, 607.
(15) Sundberg, E. J.; Sundberg, D. C. *J. Appl. Polym. Sci.* **1993**, *47*, 1277.
(16) Daniels, E. S.; Dimonie, V. L.; El-Aasser, M. S.; Vanderhoff, J. W. *J. Appl. Polym. Sci.* **1990**, *41*, 2463.
(17) Chen, Y.-C.; Dimonie, V.; El-Aasser, M. S. *J. Appl. Polym. Sci.* **1992**, *45*, 487.
(18) Chen, Y.-C.; Dimonie, V.; El-Aasser, M. S. *Pure Appl. Chem.* **1992**, *64*, 1691.
(19) Chen, Y.-C.; Dimonie, V. L.; Shaffer, O. L.; El-Aasser, M. S. *Polym. Int.* **1993**, *30*, 185.
(20) Muscato, M. R.; Sundberg, D. C. *J. Polym. Sci., Part B: Polym. Phys.* **1991**, *29*, 1021.
(21) Jönsson, J.-E. L.; Hassander, H.; Jansson, L. H.; Törnell, B. *Macromolecules* **1991**, *24*, 126.
(22) Jönsson, J.-E.; Hassander, H.; Törnell, B. *Macromolecules* **1994**, *27*, 1932.
(23) Okubo, M.; Katsuta, Y.; Matsumoto, T. *J. Polym. Sci., Polym. Lett. Ed.* **1980**, *18*, 481.
(24) Min, T. I.; Klein, A.; El-Aasser, M. S.; Vanderhoff, J. W. *J. Polym. Sci., Polym. Chem. Ed.* **1983**, *21*, 2845.
(25) Hergeth, W.-D.; Bittrich, H.-J.; Eichhorn, F.; Schlenker, S.; Schmutzler, K.; Steinau, U.-J. *Polymer* **1989**, *60*, 1913.
(26) Perrin, F. *J. Phys. Radium* **1934**, *Serie VII, V(10)*, 497.
(27) Van Krevelen, D. W. *Properties of Polymers*; Elsevier: Amsterdam, 1990; Chapters 15, 16.
(28) Broseta, D.; Leibler, L.; Kaddour, L. O.; Strazielle, C. *J. Chem. Phys.* **1987**, *87*, 7250.
(29) Kurata, M.; Tsunashima, Y.; Iwama, M.; Kamada, K. In *Polymer Handbook*, 2nd ed.; Brandrup, J., Immergut, E. H., Eds.; Wiley-Interscience: New York, 1975; Chapter IV.
(30) Siow, K. S.; Patterson, D. *J. Phys. Chem.* **1973**, *77*, 356.
(31) Walling, C. *Free Radicals in Solution*; Wiley-Interscience: New York, 1957.
(32) Lee, D. I.; Ishikawa, T. *J. Polym. Sci., Polym. Chem. Ed.* **1983**, *21*, 147.
(33) Daniel, J. C. *Makromol. Chem. Suppl.* **1985**, *10/11*, 359.

MA950512B